EFFECT OF GRAPHENE QUANTUM DOTS ON HEALTH AND ENVIRONMENT: IMPLICATIONS FOR EVERYDAY LIFE

Kanwar Abhay Singh

Department of Biotechnology and Medical Engineering

National Institute of Technology Rourkela

EFFECT OF GRAPHENE QUANTUM DOTS ON HEALTH AND ENVIRONMENT: IMPLICATIONS FOR EVERYDAY LIFE

A thesis submitted in partial fulfilment

of the requirements for the degree of

Master of Technology

in

Biotechnology

By

Kanwar Abhay Singh

215BM2258

based on research carried out

under the supervision of

Dr. Sirsendu Sekhar Ray

Department of Biotechnology & Medical Engineering

National Institute of Technology Rourkela-769008, Orissa, India

2017

Department of Biotechnology and Medical Engineering
National Institute of Technology Rourkela

May 31,2017

Prof. Sirsendu Sekhar Ray
Professor

Supervisors' Certificate

This is to certify that the work presented in the dissertation entitled "*Effect Of Graphene Quantum Dots On Health And Environment: Implications For Everyday Life* "submitted by *Kanwar Abhay Singh*, Roll Number 215BM2258, is a record of original research carried out by him under our supervision and guidance in partial fulfilment of the requirements of the degree of *M.Tech Biotechnology* in *Department of Biotechnology and Medical Engineering*. Neither this dissertation nor any part of it has been submitted earlier for any degree or diploma to any institute or university in India or abroad.

Dr. Sirsendu Sekhar Ray

Assistant Professor

Department of Biotechnology and Medical

Engineering

National Institute of Technology, Rourkela

Declaration of Originality

I, *Kanwar Abhay Singh*, Roll Number *215BM2258* hereby declare that this dissertation entitled "*Effect Of Graphene Quantum Dots On Health And Environment: Implications For Everyday Life"* presents my original work carried out as a Masters student of NIT Rourkela and, to the best of my knowledge, contains no material previously published or written by another person, nor any material presented by me for the award of any degree or diploma of NIT Rourkela or any other institution. Any contribution made to this research by others, with whom I have worked at NIT Rourkela or elsewhere, is explicitly acknowledged in the dissertation. Works of other authors cited in this dissertation have been duly acknowledged under the sections "Reference" or "Bibliography". I have also submitted my original research records to the scrutiny committee for evaluation of my dissertation.

I am fully aware that in case of any non-compliance detected in future, the Senate of NIT Rourkela may withdraw the degree awarded to me on the basis of the present dissertation.

Kanwar Abhay Singh

May 31, 2017

Acknowledgement

This project would remain incomplete if I fail to acknowledge some very important people who have been a great source of inspiration, support and guidance to me throughout. Firstly, I would like to express my heartfelt gratitude towards my highly motivating and extremely supportive supervisor **Dr. Sirsendu Sekar Ray** , Department of Biotechnology and Medical Engineering for giving me an opportunity to carry out this project work and for standing by me at every step.

I would like to thank Head of the Department of Biotechnology and Medical Engineering, National Institute of Technology Rourkela for the support. I am grateful to the Department of Ceramic Engineering, the Department of Mining, the Department of Physics and Department of Life Science for permitting me to use their facilities and infrastructure.

I am thankful to my **faculty members, technical staff** and my **parents** for their support and encouragement .

Abstract

Organic nanomaterials are carbon-based materials, which have dimensions in the range of 10^{-9} metres and are being utilised in a myriad of commercial applications. Quantum dots are unique particles with the size less than 10 nm. These particles have found to have excellent physicochemical properties as well as photolumincent abilities. However, the effect of continuous exposure to these particles has not been studies. Furthermore, more the production of these GQD from sources such as cigarette ash or fuel exhaust has not been reported.

In this work we have attempted to understand the effect the of long-term effect of exposure to the GQD by estimating the in vitro cytotoxicity of the GQD by assays such as MTT, TBARS, ROS generation and the effect on protein misfloding over a period longer than hours.

Further, we have tried to understand the effect that these particles have on the natural environment in terms of their effect on freezing point depression of water, the effect of the GQD on the biofilm formation as and health effects such as calcification of the arteries due to aggregation of calcium salts on the GQD particles.

Key words : quantum dots , Cytotoxicity.

Contents

Supervisors' Certificate ii

Declaration of Originality iii

Abstract v

List of tables: xi

Chapter 1 1

Introduction 1

Chapter 2 3

Literature survey 3

Chapter 3 7

Materials and methods 7

3.1. Characterisation and in vitro cytotoxicity of Graphene quantum dots: 7

3.1.1Extraction process: 7

3.1.1 TEM: 7

3.1.2 XRD: 7

3.1.3 FTIR: 8

3.1.4 Zeta Potential: 8

3.1.6 Spectrofluorimetry: 8

3.1.7 Biofilm formation assay: 8

3.1.8 MTT assay: 8

3.1.9 TBARS Assay: 9

3.1.10 Confocal Microscopy: 9

3.1.11 Circular Dichroism: 10

3.2 Characterization and Environmental Effect of GQD 10

3.2.1 Synthesis and characterization of lab generated GQD: 10
3.2.3 Preparation and characterization of Pickering emulsion using GQD : 10
3.2.3 Differential scanning calorimetry and freezing analysis of GQD: 10
3.2.4 GQD induced calcification: 11
3.2.5 Vapour phase extraction of GQD: 11
Chapter 4 12
Results and discussions 12
4.1 Characterization and Cytotoxicity of Cigarette derived GQD 12
4.1.1 Isolation of GQD from isolated Cigarette Ash: 12
4.1.2 TEM: 12
4.1.3 XRD 13
4.1.4 FTIR 14
4.1.5 UV Visible spectroscopy 15
4.1.6 Fluorescence Spectrofluorimetry: 16
4.1.7 Determination of Cell viability using MTT 16
4.1.8 Determination of ROS generation using H2DCFDA 17
4.1.9 TBARS Assay 18
4.1.10 Effect on protein misfolding 19
4.2 Characterization and *in vitro* Cytotoxicity of Exhaust derived GQD 20
4.2.1. TEM 20
4.2.2 XRD 21
4.2.3 FTIR 22
4.2.4 UV Visible spectroscopy 23
4.2.5 Fluorescence Spectrofluorimetry: 24
4.2.6 Determination of Cell viability using MTT: 24
4.2.7 Determination of ROS generation using H2DCFDA 25

4.2.8 TBARS Assay 26
4.2.9 Effect on protein misfolding: 27
4.2.10 Effect on Biofilm formation 28
4.3 Environmental and long term health impact of GQD 29
4.3.1 Characterization of Lab synthesized GQD: 29
4.3.2 GQD stabilized Emulsions: 30
4.3.3 DSC and Freezing analysis of GQD solutions: 31
4.3.4 GQD induced calcification: 33
Chapter 5 35
Conclusion 35
Chapter 6 36
References 36

List of figures

Figure 3-1 (a)&(b) schematic diagram of Cryoprobe set up; (c) live image of the set up **11**

Figure 4-2 HR tem images of cigarette GQD. **13**

Figure 4-3 XRD of cigarette derived GQD **14**

Figure 4-4FTIR of Cigarette GQD **15**

Figure 4-5 PL spectra of cigarette derived GQD **16**

Figure 4-6: MTT of Cigarette GQD **17**

Figure 4-7 ROS generation in Cigratte GQD using H2DCFDA **18**

Figure 4-8 TBARS assay of Cigarette derived GQD **19**

Figure 4-9 CD spectra of cigarette derived GQD treated with lysozyme **20**

Figure 4-10 HR tem images of petrol GQD. **21**

Figure 4-11 XRD petrol GQD **22**

Figure 4-12 FTIR petrol GQD **23**

Figure 4-13 UV visible spectroscopy petrol GQD **23**

Figure 4-14 PL spectra of petrol derived GQD **24**

Figure 4-15 MTT assay of petrol GQD **25**

Figure 4-16 ROS generation of petrol GQD using H2DCFDA **26**

Figure 4-17 TBARS assay of Petrol GQD **27**

Figure 4-18 CD spectra of GQD treated lysozyme **28**

Figure 4-19 Effect of petrol GQD on biofilm formation **29**

Figure 4-20 Physical characterization of GQD ;(a) HR TEM ;(b) UV Visible spectroscopy ;(c) FTIR of the GQD;(d) SAED analysis of the GQD ;(e) XRD diffract gram of the GQD; (f) PL spectra of the GQD **30**

Figure 4-21 (a) Emulsion formed by using different concentration of GQD (50,20,10,5,1,0 mg/ml from right to left respectively); (b) E-SEM micrographs of the GQD stabilised emulsion ; (c)Confocal microscopy images of the Emulsions **30**

Figure 4-22 Stability analysis of the emulsions (a) variation in size of droplet with increasing GQD concentration;(b) Variation in size of droplets with changing centrifugation speeds ; (c) Variation in size of droplets with changing

centrifugation time;(d) change in opacity with carrying GQD concentration;(e) change in opacity with change in centrifugation time. **31**
Figure 4-23 DSC graphs of GQD solutions with water as control **32**
Figure 4-24 Temperature vs Time graphs obtained by using cryoprobe set up (a) and (b) constant time experiments ;(c) and (d) constant temperature experiments **33**
Figure 4-25 (a)&(b) SEM image and EDAX graph respectively of control PDMS film; (c)&(d) the SEM image and EDAX graph of the GQD coated samples. **33**
Figure 4-26 :(a) Vapour Phase extraction set up ; (b) extraction in ACN ; (c) extraction in Butanol ; (d) extraction in Chloroform **34**

List of tables:

Table 2-1 Cytotoxicity based on the method of preparation of lab synthesised GQD [9] 4

Table 2-2 Comparison of GQD cytotoxicity on various cell lines[9] 6

Chapter 1

Introduction

The role of nanoparticles in biological application has undergone a drastic change, with a variety of them synthesised for specific purposes such as bio imaging, targeted binding to cellular components for the purposes of tagging cells as well the use of a variety nanomaterials such as Carbon nanotubes and its functionalised variants used extensively in the field of tissue engineering. Their unique surface properties as well as the ease with which the can be tailored at an elemental level has resulted in the generation of a wide variety of chemically unique particles designed to perform a specific function. While the scientific community as a whole has recently obtained the technological expertise as well as equipment to synthesise, characterise nanoparticles, the spreads of these technologies have led to the a rather odd conclusion; that we are not the first to create unique structures at Nano level, as always nature proved itself superior to the innovations of man. From the nanolayers in the shells of certain mollusc to the nonporous of certain clay there exist whole hosts of various naturally occurring nanoparticles that are involved in key environmental process.

However, with the spread of the technology necessary for isolation and characterization of nanoparticles, the list of industrial processes that release nanoparticles has grown exponentially, a particularly alarming addition being the release of nanoparticles form the combustion of fossil fuels. To the understand the true gravity of this development we must consider the sheer volume of exhaust being generated from the burning of these fuels and the concentration of particles being generated. Analysis of fuel exhaust has shown the presence has shown the presence of carbon nanoparticles of varying sizes, which are then released into the general environment. The release of varying sizes of nanoparticles becomes an even more important discovery when viewed in conjugation with existing data on nanoparticles cytotoxicity, which points towards a correlation between the sizes, elemental composition with the toxicity of nanoparticles

The present study deals with the isolation of the GQD from unreported sources such as cigarette ash and exhaust fumes followed the estimation of the cytotoxicity of these GQD via techniques such as MTT assay, TBARS assay and estimation of ROS generation. We further determined the effect these GQD would have on protein folding by determining the change in the secondary structure of the protein after exposure to the GQD. Lastly, we attempted to understand the long-term effect of GQD accumulation both in the environment and in the human body by analysing their ability to cause depression in freezing point of aqueous solution and their effect on increased calcification in the coronary artery respectively.

Chapter 2

Literature survey

There are primarily two methods for creation GQDs (graphene quantum dots) top down approaches or bottom up approach. The top down approach deals with disrupting or slicing of larger bulk materials to prepare the nanomaterials. In case of GQDs, the bulk material generally is either graphite or graphene oxide. A variety of physical processes can be for the purpose of such as Oxidative cutting, microwave assisted cutting, hydrothermal cutting, physical and electrochemical exfoliation. On the other hand, bottom up approaches deal with the clustering of individual atoms in order to form the GQD. Bottom up approach includes methods such as pyrolysis, hydrothermal synthesis. Table 2-1 summarizes the literature correlating the synthesis methods and the cell viability.

Synthesis type	**Synthesis method**	**Cell type/ Viability(%)**	**Reference**
Top down	Photo-Fenton assisted cutting of GO	85%/MCF-7	[1]
Top down	Oxidation cutting of graphite	76%/A549	[2]
Top down	Oxidation cutting of graphite	95%/Hela, 93%/A549	[3]
Top down	Microwave assisted cutting of GO	99%/Hela	[4]
Top down	Hydrothermal cutting graphite in oxidizers	84%/THP1	[5]

Top down	Electrochemical exfoliation of graphite rod	76%/U251	[6]
Top down	Exfoliation of carbon fibre in mixed acids	78%/A549, 76%/KB	[7]
Bottom up	Pyrolysis of citric acid	92%/A549	[3]
Bottom up	Pyrolysis of L-glutamic acid		[8]
Bottom up	Alkali-mediated hydrothermal treatment of pyrene	61%/stem cells	[9]

Table 2-1 Cytotoxicity based on the method of preparation of lab synthesised GQD [9]

Another major factor the effects the toxicity analysis of the GQDs is the type of cell line used for the *in vitro assays.* Certain cell lines such as cancerous cell lines are more resistant to GQD as compared to mortal cell lines. The duration of exposure is another key factor in the overall determination of cell toxicity. For use in fields that involve prolonged exposure to the GQD such as bioimaging, the GQD must be nontoxic for a considerable time.

The most common assays used in the estimation of the in vitro cytotoxicity are:

- MTT : Which deals with the effect of the GQDs on the cells metabolic activity
- LDH: which deals with estimation of the integrity of the plasma membrane
- Comet Assay : To determine Geno toxicity

A brief summary of the work done in cytotoxicity of GQD can be seen in Table 2-2 which list the major works done in the field of GQD synthesis along with the type of cell line used and duration of exposure to the GQD

Cells for tests	GQDs	Assays	Toxicity	Incubation time	Ref
MCF-7, Hela cells, MCF-10A	GQDs	MTT	95% via. at 2 mg mL^{-1}	24 h	[10]
Hela, A549 cells	GQDs	MTT, LDH	Via. > 95% at 160 μg mL^{-1} (Hela); Via. > 85% at 640 μg mL^{-1}(A549)	24 h	[11]
Hela cells	GQDs	CKK-8	90% via. at 100 μg mL^{-1}	24 h	[12]
A549 cells	GQDs	MTT	Via. > 80% at 200 μg mL^{-1}	24 h	[13]
KB, MDA-MB231, A549, MDCK cells	GQDs	MTT, LDH	Via. > 95% at 500 μg mL^{-1} (MDCK cell)	21 d/24 h	[14]
A549 cells	GQDs	MTT	80% via. at 100 μg mL^{-1}	24 h	[15]
MGC-803, MCF-7 cells	GQDs	MTT	GQDs < GO	3 d	[16]
Stem cells	GQDs	MTT	Via. > 70% at 200 μg mL^{-1}	24 h	[17]

Stem cells	GQDs	MTT	61% via. at 100 μg mL^{-1}	24 h	[18]
THP-1 macrophages	GQDs	MTT	82.5% via. at 200 μg mL^{-1}	24 h	[19]
MG-63 and MC3T3 cells	GQDs	MTT	Via. > 80% at 400 μg mL^{-1}	24 h	[20]
RSC96	GQDs	MTT	70% via. at 200 μg mL^{-1}	24 h	[21]
Hela cells	bGQD	MTT	87% via. at 4.0 mg mL^{-1}	12 h	[22]

Table 2-2 Comparison of GQD cytotoxicity on various cell lines[9]

Chapter 3

Materials and methods

3.1. Characterization and in vitro cytotoxicity of Graphene quantum dots:

3.1.1Extraction process:

The petrol exhaust was passed through a vessel containing distilled water via a system of pipes; the process was run for a long duration of time in order obtain a significant amount of nanoparticles. The distilled water containing nanoparticles obtained from this process was then subjected to a two-step centrifugation process in order to segregate the nanoparticles. The first step was centrifugation at 2000 rpm in order to remove any suspended soot particles, followed by a second; high speed centrifugation at 8100 g in order to segregate the nanoparticles based on their size.

3.1.1 TEM:

The transmission electron microscope was used to determine the size and structure of the isolated GQD. The Elemental composition was determined using EDAX and elemental distribution was judged by using HADDAF. Finally, the crystallinity was determined using the SAED. Samples were dispersed in water then loaded on to the carbon coated copper TEM grids.

3.1.2 XRD:

The X-Ray Diffraction XRD analysis was carried out to understand the crystallinity of the of the isolated nanoparticles. This analysis also allows us to differentiate the GQD from common soot generated by the in complete burning of fuels (the later having high amorphous peaks).

3.1.3 FTIR:

To understand the nature of the chemical bonds present on the surface of the GQD FTIR analysis was performed using a Perkin Elmer Spectrum 2. Samples were prepared by adding a small quantity of dried GQD to Potassium bromide (KBr) and then mixing in a mortar till a homogenous mixture is achieved. This mixture was then placed in a mechanical press and the film thus formed is placed into the machine for analysis Scans were conducted from 400 cm^{-1} to 4000 cm^{-1}.

3.1.4 Zeta Potential:

The zeta potential was used to determine the stability of the GQD in an aqueous system . This was essential as all *in vitro* assays would be occurring in aqueous environments.. The zeta potential was determined by using a Malvern nano ZS

3.1.6 Spectrofluorimetry:

Determine the PL spectra of the GQD, fluorescence spectroscopy was performed using the perkin elmer LS-55. Samples were subjected to excitation wavelength ranging from 250 to 800 nm.

3.1.7 Biofilm formation assay:

Biofilm formation was by using crystal violet staining protocol . Overnight grown cultures of *E.coli* and *B.subtilis* were incubated with the nanoparticles at varying concentration in test tubes for a period of 3 days at 37^0C. After which, media was decanted and the tubes were stained with 0.1% crystal violet. The excess stain was the removed by washing with distilled water and the adhered stain was solubilized in iso-propanol and concentration was crystal violet was determined by measuring the absorbance 595nm.

3.1.8 MTT assay:

HeLa cells were seeded in a 96-well cell culture plate in Dulbecco's modified Eagle medium (DMEM) at a density of 5 × 104 cells mL−1 with 10% fetal bovine serum (FBS) at 37 °C and with 5% CO2 for 24 h. After which they were replaced with media containing different concentration of GQDs and cultured for another 24 hours (1 day), 72 hours (3 days) respectively. Then, 20 μL of 5 mg mL−1 MTT (3-(4,5-

dimethylthiazol-2yl)-2,5-diphenyltetrazolium bromide) solution was added to every cell well. The cells were further incubated for 3 hours, followed by removal of the culture medium with MTT, and addition of 200 μL of DMSO. The resulting mixture was shaken for 15 min at room temperature. The absorbance of MTT at 595 nm was measured on an automatic ELISA analyzer (SPR-960). The control data were obtained in the absence of nanoparticles.

3.1.9 TBARS Assay:

The MDA content, a measure of lipid peroxidation, was assayed in the form of thiobarbituric acid reactive substance (TBARS) (Ohkawa et al., 1979). HEK293 cells were plated into a 24-well plate at a density of 1.0 105 cells/well. After 24 h exposure to nanoparticles, the cells were washed with ice-cold PBS and lysed using lysis buffer. The cell homogenates were used in the TBARS assay. Briefly, 100 uL cell homogenates were mixed with 1 ml of 0.67% TBA, 1.5 ml 20% trichloroacetic acid, and 1.5 ml 0.04% BHT in test tubes. The mixtures were incubated in a boiling water bath for 20 min. After cooling to room temperature, the reaction mixture was centrifuged at 4000g for 10 min and the absorbance of the supernatant was measured at 530nm using the same mutli-well plate reader.

3.1.10 Confocal Microscopy:

RAW cells cultured in DMEM containing 1g/L glucose, 10% FBS and antibiotics were seeded on a glass cover slip at a density of 104 cells per slip and incubated at 37˚C under 5% CO2 conditions. The GQDs containing solution obtained was filtered autoclaved and added over the cells while maintaining the ratio of carbon dot solution to media at 200 ug/ml. The cells were incubated with the GQDs for a period of 12 hours and subsequently visualised under a confocal microscope (Leica TCS). Prior to visualization, various dyes such as H2DCF DA were added to the cells to understand the effect of the GQD on the cells.

3.1.11 Circular Dichroism:

The effect of the GQD on the protein secondary structure was assed using CD spectroscopy. The GQD were mixed with Lysozyme solution (mg/ml) at varying ratios the effect on the Secondary structure was measure after hours of incubation at 2^{o}C .The data obtained was then replotted using K2D3 software to determine the secondary structures.

3.2 Characterization and Environmental Effect of GQD

3.2.1 Synthesis and characterization of lab generated GQD:

The GQD were synthesised using hydrothermal process in which 3g of dextrose was added to 40 ml of milli Q water in a Teflon container. The container was then placed inside a furnace at 180^{o}C for 3.5 hours. The GQD were analysed using TEM, XRD, FTIR, UV spectroscopy and Fluorescence spectroscopy in the manner mentioned earlier.

3.2.3 Preparation and characterization of Pickering emulsion using GQD :

The oil in water (o/w) emulsions were prepared using hexadecane and an aqueous GQD n suspension at the required concentration without further dilution. All the emulsions were prepared using an oil/aqueous phase ratio of 30/70. Practically, 0.3 mL of hexadecane was added to 0.7 mL of aqueous suspension in a plastic vial and sonicated with and ultrasonic bath sonicator at a power of 2 W/mL for 90 s. The Emulsion were analysed with the help of ESEM, Confocal and light microscopy.{Kalashnikova, 2011 #28}

3.2.3 Differential scanning calorimetry and freezing analysis of GQD:

A detailed thermal analysis of the GQD solutions of varying concentrations was done by using Differential Scanning calorimetry , The analysis was done in a temperature range of -30 to +30^{o}C at a rate of 2 degree/minute. The same solution was also used to estimate the freeze thaw curves using a cry probe set up as shown in figure.

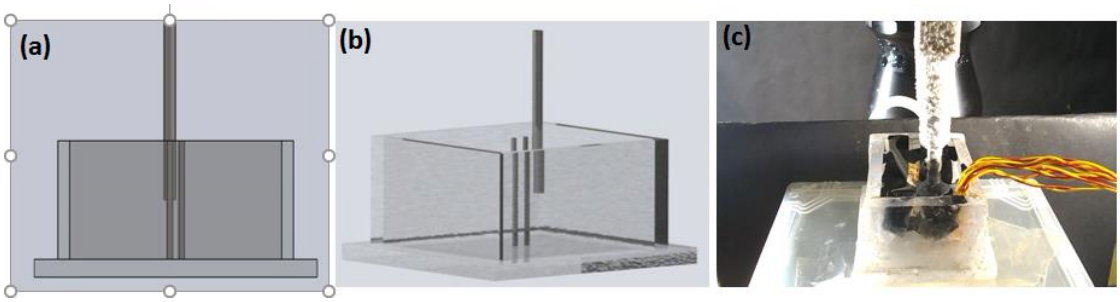

Figure 3-1 (a)&(b) schematic diagram of Cryoprobe set up; (c) live image of the set up

3.2.4 GQD induced calcification:

GQD were embedded in a PDMS layer and the placed inside a SBF (simulated body fluid) to mimic the conditions of the human body, after 72 hours the samples were observed under FESEM to visualise the calcium deposition.

3.2.5 Vapour phase extraction of GQD:

The ability of the GQD separate in the vapours phase was estimated dispersing the GQD in the solvent and heating it above it boiling point in order to obtain the vapours. These were then collected in another flask via the set shown in figure 13. The process was repeated for multiple solvents such as acetonitrile, butanol, Chloroform and hexane

Chapter 4

Results and discussions

4.1 Characterization and Cytotoxicity of Cigarette derived GQD

4.1.1 Isolation of GQD from isolated Cigarette Ash:

Ash was dissolved in distilled water and then vortexed to ensure proper mixing. The distilled water containing nanoparticles obtained from this process was then subjected to a two-step centrifugation process in order to segregate the nanoparticles. The first step was centrifugation at 2000 rpm in order to remove any suspended soot particles, followed by a second; high-speed centrifugation at 8100 g in order to segregate the nanoparticles based on their size.

4.1.2 TEM:

It was observed in earlier studies that a number of key characteristics such as physiochemical properties of nanoparticles (particularly those in termed as quantum dots) are related to the size and composition of the particles in question. Hence, the morphology of the isolated nanoparticles was studied using both Field Emission Scanning electron microscopy as well as HR TEM (high resolution transmission electron microscopy). The images showed the diameter of the nanoparticles varies between 4-15 nm, with an average diameter of 9.88nm. The lattice spacing was these particles was found to vary between 0.24 nm and 0.420 nm. We infer from literature that this variation could possibly be due change in actual elemental composition of nanoparticles in question, which is possible since the process of combustion by which they are created is not entirely uniform.

Further The HADDAF analysis indicated the presence of primarily four elements in the particles namely carbon, nitrogen, oxygen, phosphorous. This is in line with expectations since these are the major components of all organic plant matter. Lastly, SAED analysis indicated the presence of crystalline structure with interlayer spacing corresponding to those observed in the Tem micrographs.

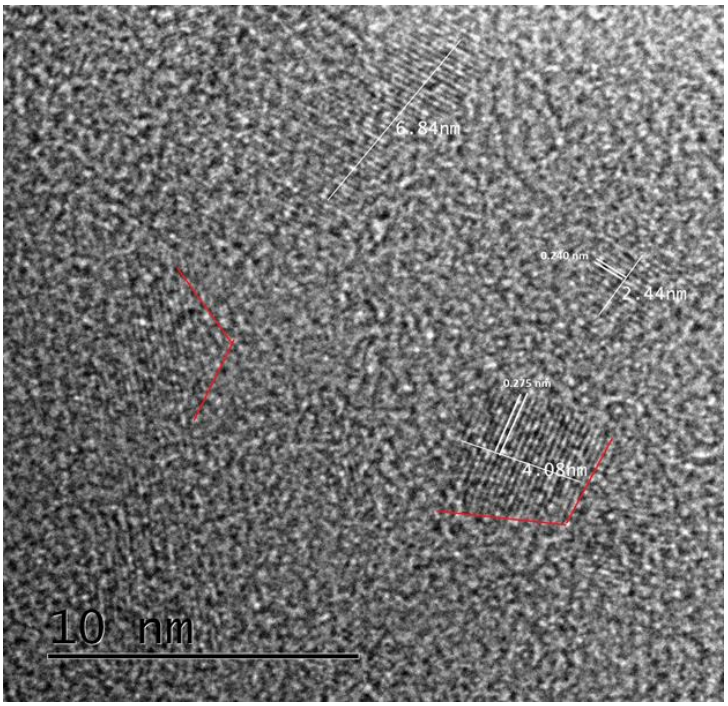

Figure 4-2 HR tem images of cigarette GQD.

4.1.3 XRD

the X ray diffractogram of the isolated nanoparticles upon further analysis we see that the particles show a set of sharp peaks in the 20 to 30 degree range, 26^0 with an interlayer spacing of 0.340 nm point towards the presence of Graphene oxide quantum dot structure.

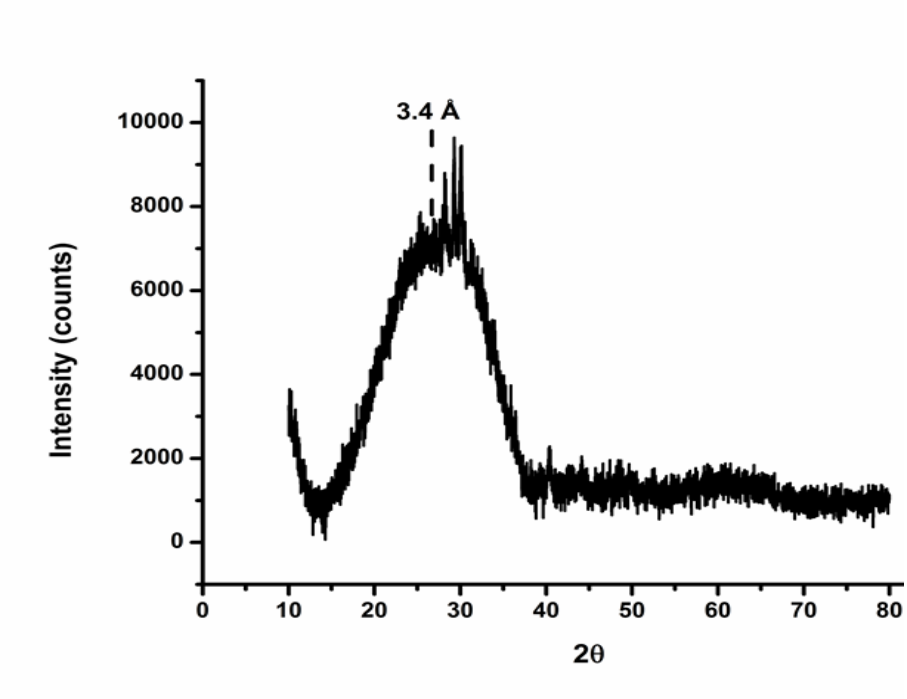

Figure 4-3 XRD of cigarette derived GQD

4.1.4 FTIR

Upon analysis of the nanoparticles using FTIR we observe a variety of high intensity peaks, most notably a characteristic peak for C=C at 1600 cm^{-1} confirming our assertion about the graphitic nature of the nanoparticles. High intensity peaks were also seen at 1400cm^{-1} which is similar to that seen in case of C-N stretching and at 3400 cm^{-1} which appear due to the presence O-H, N-H bonds. Furthermore, a set of peaks in the 1040-1140 cm-1 range can be attributed to SO^{3-}, C–O, and C–O–C bonds; In particular the shark high intensity peak at 1135 cm^{-1} can be ascribed to the C–O bond. Finally, thee cluster pf peaks in the 600-660 cm^{-1} range which signed to P═O stretching, P–C of P-aromatic stretching, P–O–C, P–OH, and P–C . The Fir analysis of the particles confirms the presence of double bonded carbon with a high of nitrogen oxygen sulphur and phosphorous atoms acting as impurities, which result in the presence of a large number of function groups being present on the surface of the particles. This further corroborates the conclusion that we derived from the X-ray diffractogram about the structure of the particles being similar to that of GQDs .

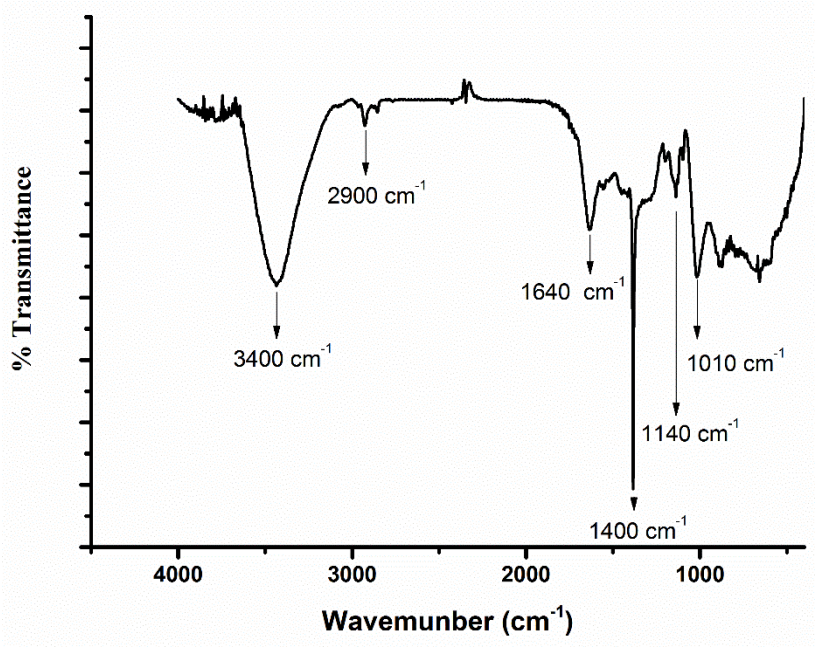

Figure 4-4FTIR of Cigarette GQD

4.1.5 UV Visible spectroscopy

These nanoparticles (hence forth referred to as GQDs) show optical absorption in the UV region, particularly near 210, with a tail extending to the visible range(Figure 3c). This absorption peak is primarily attributed to the π–π* transition of the C=C bonds,

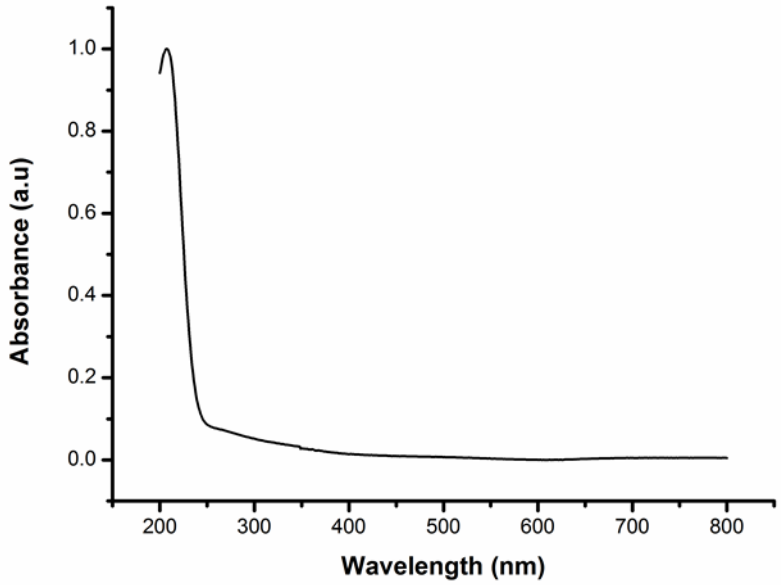

Figure 4-4 UV visible spectra of Cigarette GQD

4.1.6 Fluorescence Spectrofluorimetry:

The PL spectra of the cigarette showed a marked red shift in terms of the emission. This red shit is consistent with literature, however a slight variation in the spectra was observed at 250 nm. This variation can be attributed to the elemental dopants in the GQD such as nitrogen.

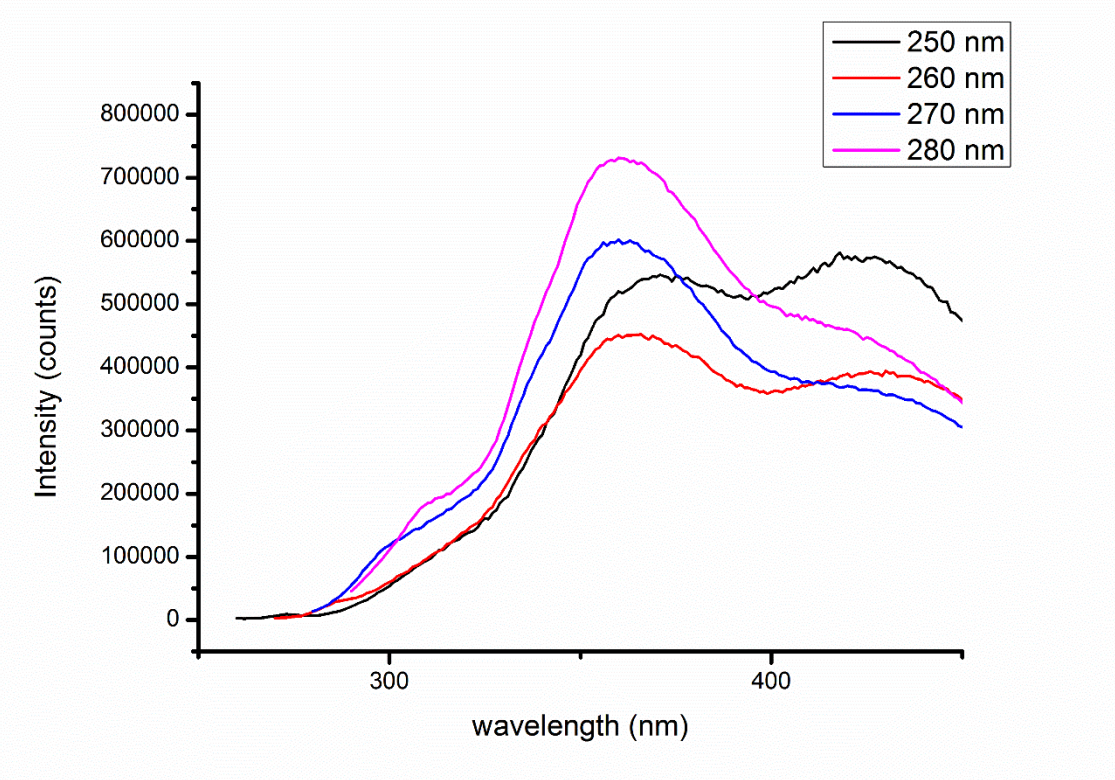

Figure 4-5 PL spectra of cigarette derived GQD

4.1.7 Determination of Cell viability using MTT

The MTT assay is used for determining the cell metabolic activity, it works on the principle of NAD(P)H-dependent cellular oxidoreductase enzymes reducing the tetrazolium dye MTT 3-(4,5-dimethylthiazol-2-yl)-2,5-diphenyltetrazolium bromide to its insoluble formazan (which has a purple colour). This colour is then measured in order to judge the extent of mitochondrial activity. The MTT assay allows us to understand the effect of the isolated GQDs on the mitochondrial activity of the cells. Furthermore, in order to more accurately mimic the effect and extent of exposure of the these GQDs in physiological environments we performed the MTT assay after 24 and 72 hours of exposure. The results (Figure 4a) show that the mitochondrial function decreases with increasing concentration of GQDs, however the drop in mitochondrial function becomes

more pronounced at longer exposure duration (72 hours). This indicates that the cytotoxic effect of the GQDs is dependent on both the concentration of exposure as well as the duration. In practical terms, it implies that persistent exposure to even moderate levels of these GQDs would be extremely detrimental for health.

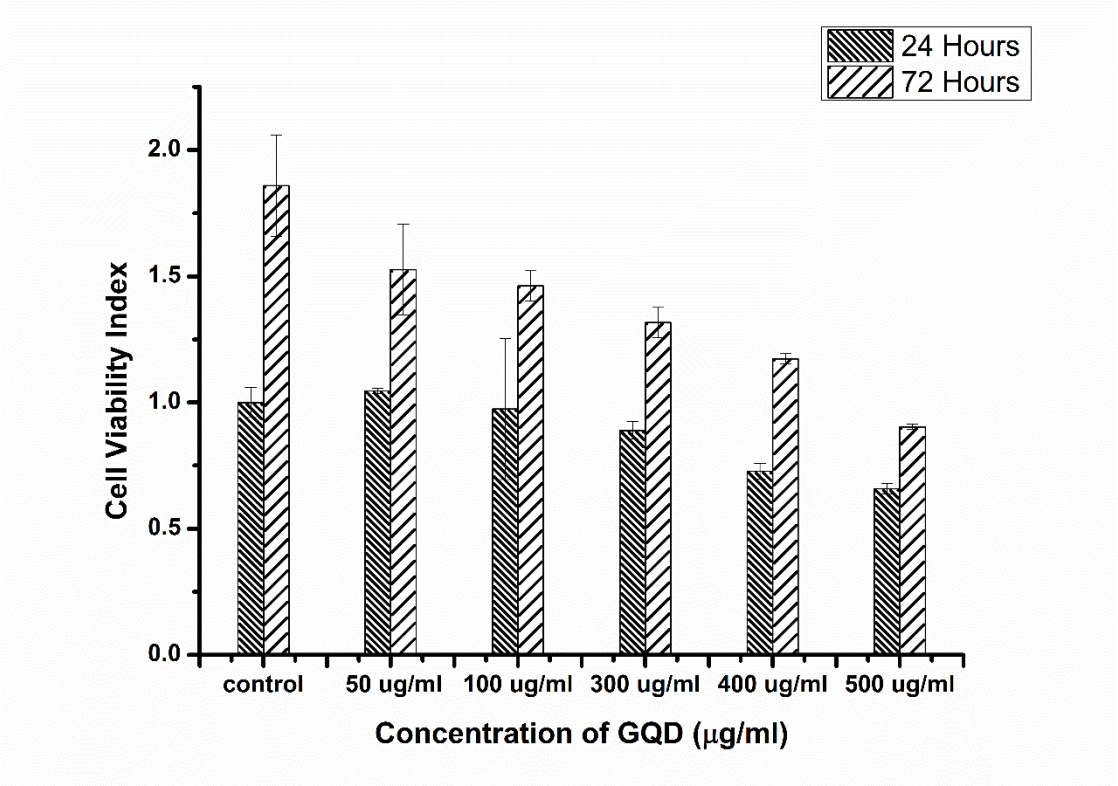

Figure 4-6: MTT of Cigarette GQD

4.1.8 Determination of ROS generation using H2DCFDA

Reactive oxygen species (ROS) is a broad term that refers to oxygen containing species such as peroxides, superoxide, and hydroxyl radical. The generation of ROS is an essential in variety of normal processes such as cell signalling and maintenance of haemostasis. However, excess generation of ROS may result in DNA fragmentation, lipid peroxidation. The ability of GQD to produce Quantum dots is well established in literature. To understand the in vitro ROS generation by the GQD we used the 2',7'-dichlorodihydrofluorescein diacetate (H_2DCFDA) dye. The cleavage of the acetate groups by intracellular esterases and oxidation, the nonfluorescent H_2DCFDA is converted to the highly fluorescent 2',7'-dichlorofluorescein (DCF). The results showed a higher amount of the ROS generation near the GQD, this can be as seen by the

localization of Green fluoresce near the GQD. O such increased aggregation was seen in the control samples.

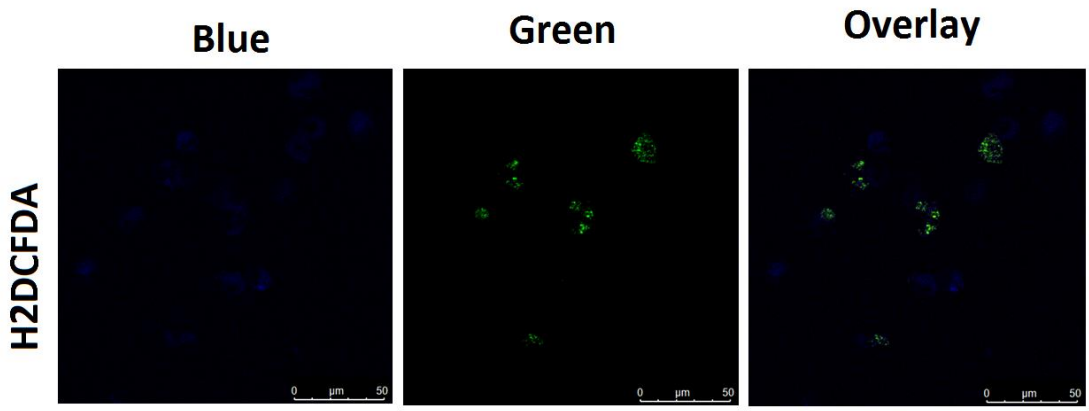

Figure 4-7 ROS generation in Cigratte GQD using H2DCFDA

4.1.9 TBARS Assay

The ability of certain nanoparticles to result in the formation of Reactive oxygen species has been determined in earlier works. To determine the produxtion of ROS generation by exhaust GQDS we have used the 2-ThioBarbituric Acid Reactive Substances (TBARS) Assay.2-ThioBarbituric Acid Reactive Substances are biomolecules that appear routinely in response to cellular oxidative stress. 2-TBARS assay results are generally expressed in the form of malonaldehyde (malondialdehyde, MDA) equivalents, a compound that results from the decomposition of polyunsaturated fatty acid lipid peroxides. The TBARS assay is an effective ,well known, established method for quantifying these lipid peroxides On exposure of nanoparticles to the HeLa cell for 24 hours it was observed the at elevated concentrations of nanoparticles (above 100 ug/mL) there is a detectable production of MDA when compared to the control sample. In particular, at concentration of 200 ug/mL it was observed the cells produced close to 1uM of MDA. This implies that even relatively low concentration, these exhaust GQDs are capable of causing lipid peroxidation, a process that results in the creation of toxic free radicals that are extremely harmful to cell.

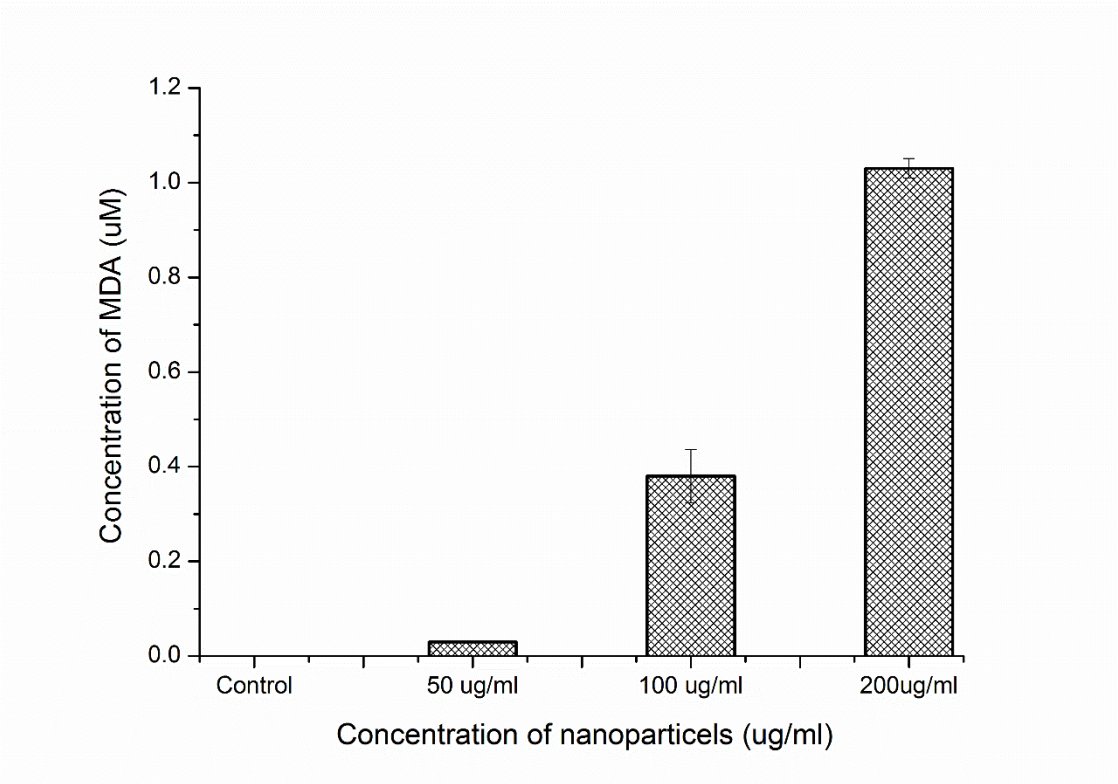

Figure 4-8 TBARS assay of Cigarette derived GQD

4.1.10 Effect on protein misfolding

The GQD also showed detrimental physiological activity when they were incubated with proteins at room temperature at varying concentrations. The results showed that GQD cause protein misfolding in particular they caused a decrease in the percentage of the alpha helical structure in the lysozyme protein. This decrease in percentage alpha increased with increase in concentration of the GQD .

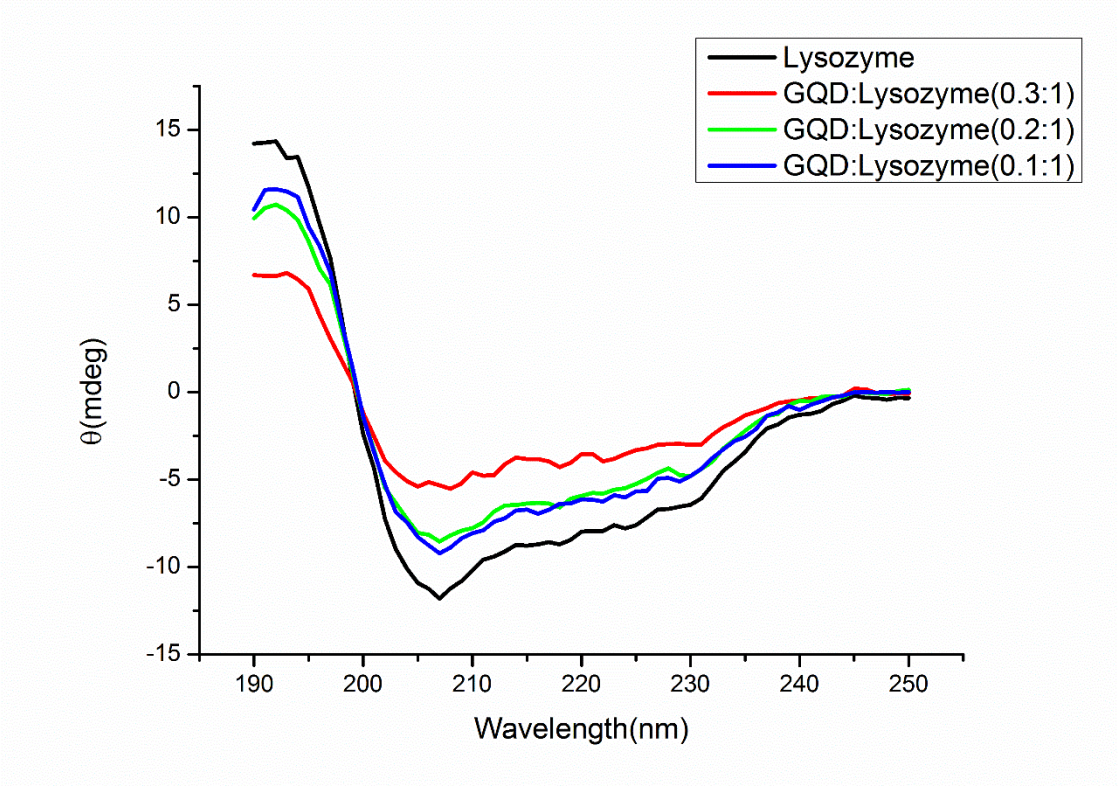

Figure 4-9 CD spectra of cigarette derived GQD treated with lysozyme

4.2 Characterization and *in vitro* Cytotoxicity of Exhaust derived GQD

4.2.1. TEM

It was observed in earlier studies that a number of key characteristics such as physiochemical properties of nanoparticles (particularly those in termed as quantum dots) are related to the size and composition of the particles in question. Hence, the morphology of the isolated nanoparticles was studied using both Field Emission Scanning electron microscopy as well as HR TEM (high resolution transmission electron microscopy). The images showed the diameter of the nanoparticles varies between 4-15 nm, with an average diameter of 9.88nm. The lattice spacing was these particles was found to vary between 0.24 nm and 0.420 nm. We infer from literature that this variation could possibly be due change in actual elemental composition of nanoparticles in question, which is possible since the process of combustion by which they are created is not entirely uniform.

Further The HADDAF analysis indicated the presence of primarily four elements in the particles namely carbon, nitrogen, oxygen, phosphorous. This is in line with expectations since these are the major components of all organic plant matter. Lastly, SAED analysis indicated the presence of crystalline structure with interlayer spacing corresponding to those observed in the Tem micrographs.

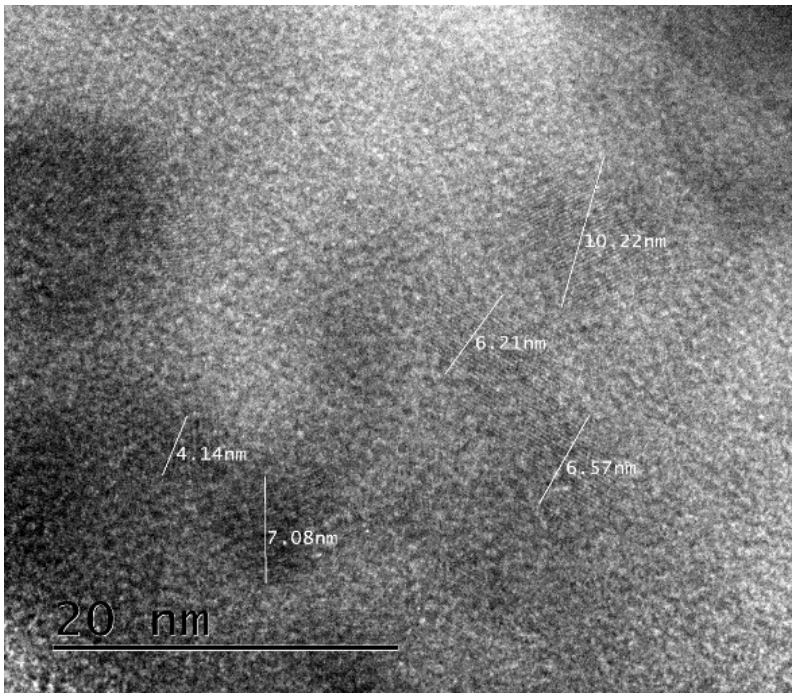

Figure 4-10 ***HR tem images of petrol GQD.***

4.2.2 XRD

the X ray diffractogram of the isolated nanoparticles upon further analysis we see that the particles show a set of sharp peaks in the 20 to 30 degree range, 26^0 (Figure 4-10) with an interlayer spacing of 0.340 nm point towards the presence of Graphene quantum dot structure.

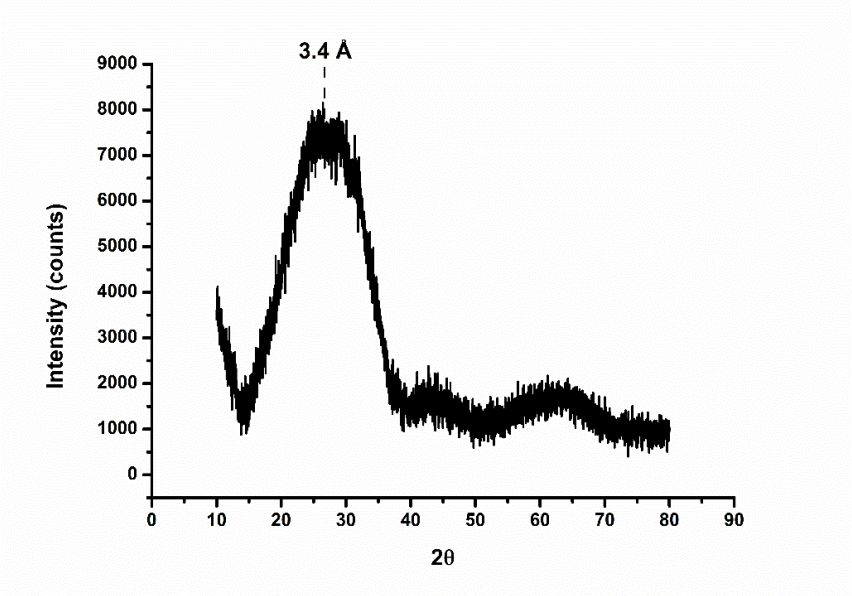

Figure 4-11 XRD petrol GQD

4.2.3 FTIR

Upon analysis of the nanoparticles using FTIR we observe a variety of high intensity peaks, most notably a characteristic peak for C=C at 1600 cm^{-1} (Peng et.al 2012) confirming our assertion about the graphitic nature of the nanoparticles. High intensity peaks were also seen at 1400cm^{-1} which is similar to that seen in case of C-N stretching and at 3400 cm^{-1} which appear due to the presence O-H, N-H bonds. Furthermore, a set of peaks in the 1040-1140 cm-1 range can be attributed to SO^{3-}, C–O, and C–O–C bonds , In particular the shark high intensity peak at 1135 cm^{-1} can be ascribed to the C–O bonds (Figure 4-11). Finally, thee cluster pf peaks in the 600-660 cm^{-1} range which signed to P═O stretching, P–C of P-aromatic stretching, P–O–C, P–OH, and P–C. The Fir analysis of the particles confirms the presence of double bonded carbon with a high of nitrogen oxygen sulphur and phosphorous atoms acting as impurities, which result in the presence of a large number of function groups being present on the surface of the particles. This further corroborates the conclusion that we derived from the X-ray diffractogram about the structure of the particles being similar to that of graphene quantum dots.

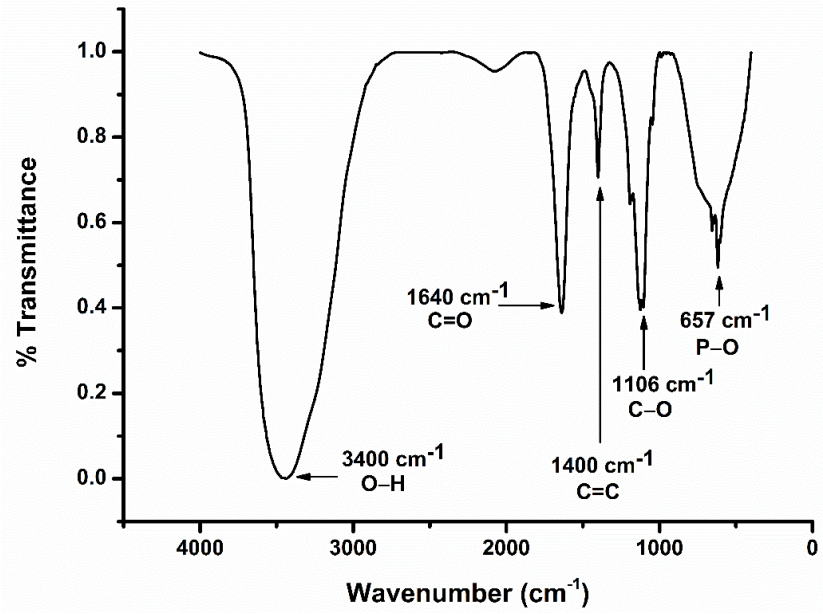

Figure 4-12 FTIR petrol GQD

4.2.4 UV Visible spectroscopy

These GQD show optical absorption in the UV region, particularly near 280nm, (Figure 4-12). This absorption peak is primarily attributed to the π–π* transition of the C=C bonds, the n–π* transition of bonds such as C=O.

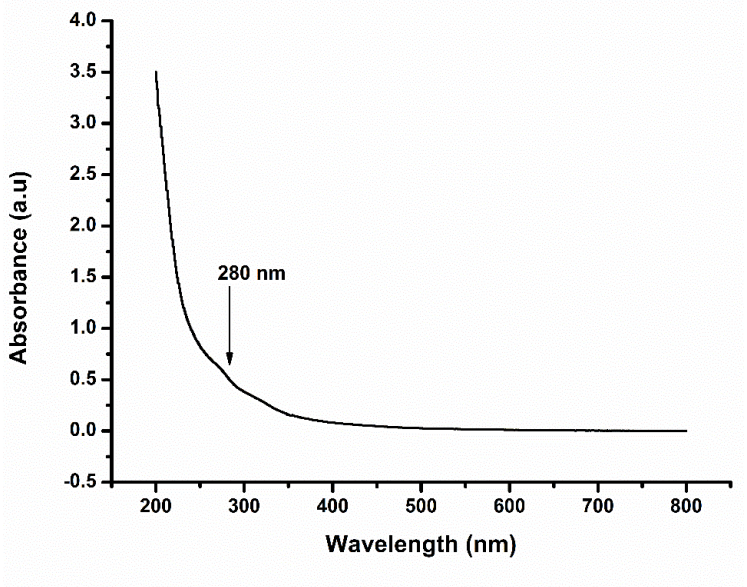

Figure 4-13 UV visible spectroscopy petrol GQD

4.2.5 Fluorescence Spectrofluorimetry:

The PL spectra of the cigarette showed a marked red shift in terms of the emission (Figure 4-13). This red shit is consistent with literature, however a slight variation in the spectra was observed at 250 nm. This variation can be attributed to the elemental dopants in the GQD such as nitrogen.

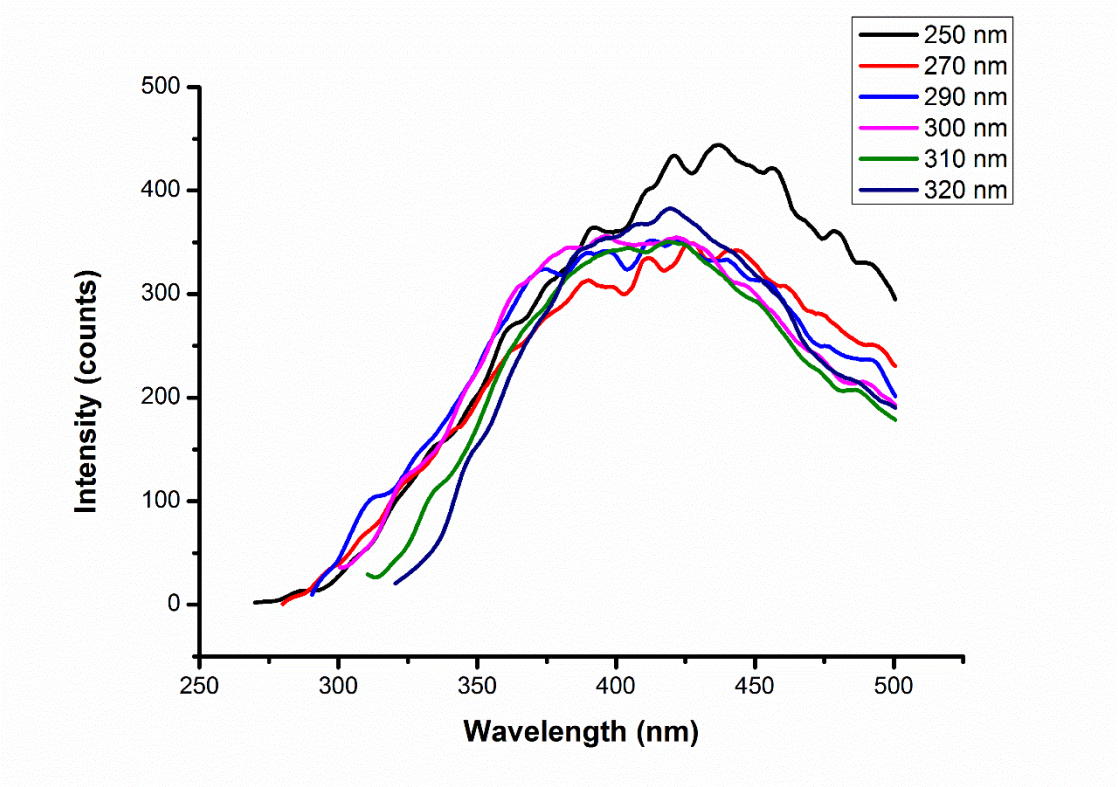

Figure 4-14 PL spectra of petrol derived GQD

4.2.6 Determination of Cell viability using MTT:

The MTT assay is used for determining the cell metabolic activity, it works on the principle of NAD(P)H-dependent cellular oxidoreductase enzymes reducing the tetrazolium dye MTT 3-(4,5-dimethylthiazol-2-yl)-2,5-diphenyltetrazolium bromide to its insoluble formazan (which has a purple colour). This colour is then measured in order to judge the extent of mitochondrial activity. The MTT assay allows us to understand the effect of the isolated GQDs on the mitochondrial activity of the cells. Furthermore, in order to more accurately mimic the effect and extent of exposure of the these GQDs in physiological environments we performed the MTT assay after 24 and 72 hours of exposure. The results (Figure 4-14) show that the mitochondrial function decreases with

increasing concentration of GQDs, however the drop in mitochondrial function becomes more pronounced at longer exposure duration (72 hours). This indicates that the cytotoxic effect of the GQDs is dependent on both the concentration of exposure as well as the duration. In practical terms, it implies that persistent exposure to even moderate levels of these GQDs would be extremely detrimental for health

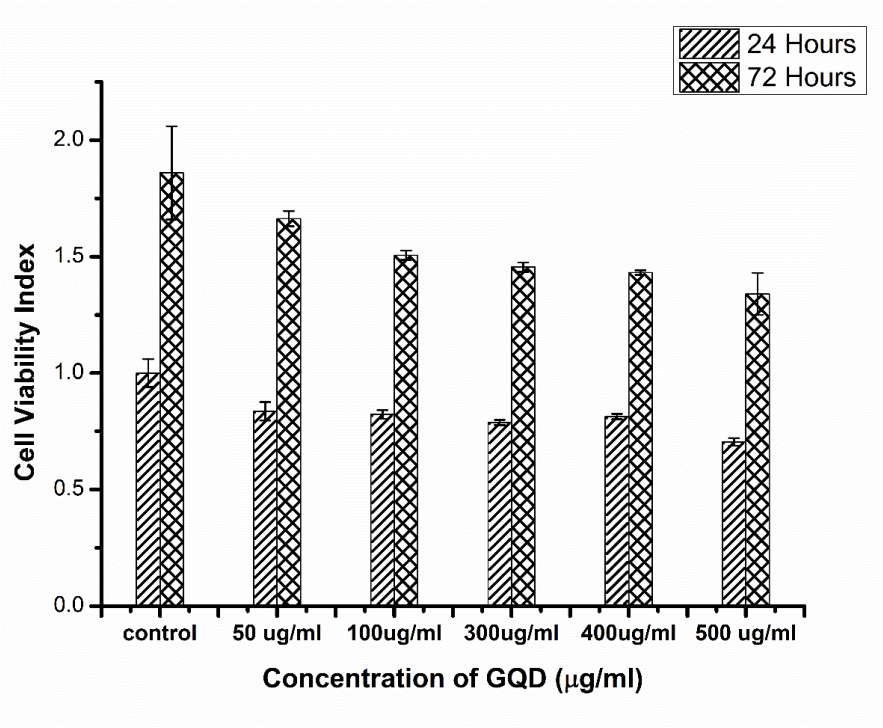

Figure 4-15 MTT assay of petrol GQD

4.2.7 Determination of ROS generation using H2DCFDA

Reactive oxygen species (ROS) is a broad term that refers to oxygen containing species such as peroxides, superoxide, and hydroxyl radical. The generation of ROS is an essential in variety of normal processes such as cell signalling and maintenance of haemostasis. However, excess generation of ROS may result in DNA fragmentation, lipid peroxidation. The ability of GQD to produce Quantum dots is well established in literature. To understand the in vitro ROS generation by the GQD we used the 2',7'-dichlorodihydrofluorescein diacetate (H_2DCFDA) dye. The cleavage of the acetate groups by intracellular esterases and oxidation, the nonfluorescent H_2DCFDA is converted to the highly fluorescent 2',7'-dichlorofluorescein (DCF). The results showed

a higher amount of the ROS generation near the GQD, this can be as seen by the localization of Green fluoresce near the GQD. O such increased aggregation was seen in the control samples.

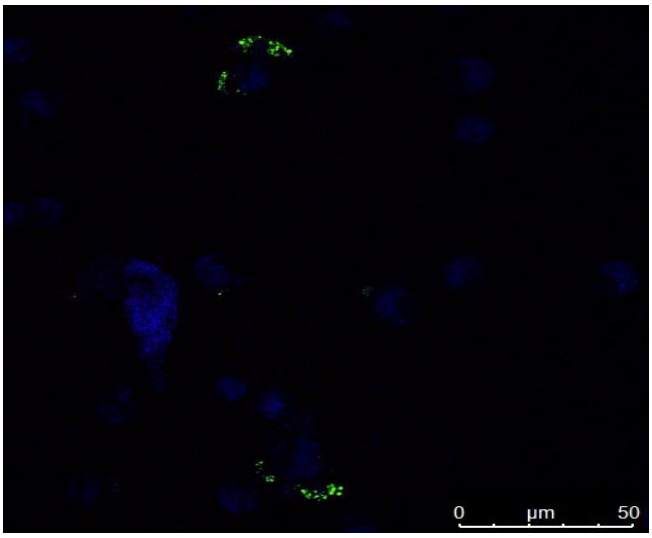

Figure 4-16 ROS generation of petrol GQD using H2DCFDA

4.2.8 TBARS Assay

The ability of certain nanoparticles to result in the formation of Reactive oxygen species has been determined in earlier works. To determine the produxtion of ROS generation by exhaust GQDS we have used the 2-ThioBarbituric Acid Reactive Substances (TBARS) 2-ThioBarbituric Acid Reactive Substances are biomolecules that appear routinely in response to cellular oxidative stress. 2-TBARS assay results are generally expressed in the form of malonaldehyde (malondialdehyde, MDA) equivalents, a compound that results from the decomposition of polyunsaturated fatty acid lipid peroxides. The TBARS assay is an effective ,well known, established method for quantifying these lipid peroxides On exposure of nanoparticles to the HeLa cell for 24 hours it was observed the at elevated concentrations of nanoparticles (above 100 ug/mL) there is a detectable production of MDA when compared to the control sample (Figure 4-16). In particular, at concentration of 200 ug/mL it was observed the cells produced close to 1uM of MDA. This implies that even relatively low concentration, these exhaust GQDs are capable of causing lipid peroxidation, a process that results in the creation of toxic free radicals that are extremely harmful to cell.

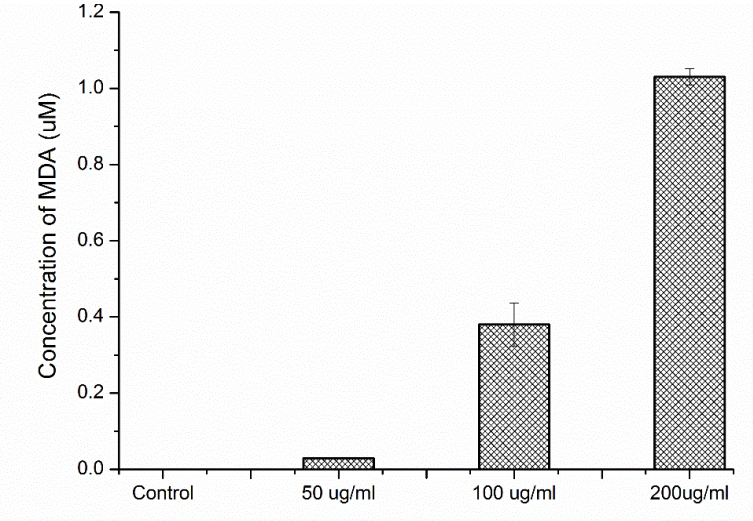

Figure 4-17 TBARS assay of Petrol GQD

4.2.9 Effect on protein misfolding:

The GQD also showed detrimental physiological activity when they were incubated with proteins at room temperature at varying concentrations. The results showed that GQD cause protein misfolding in particular they caused a decrease in the percentage of the alpha helical structure in the lysozyme protein (Figure 4-17). This decrease in percentage alpha increased with increase in GQD concentration.

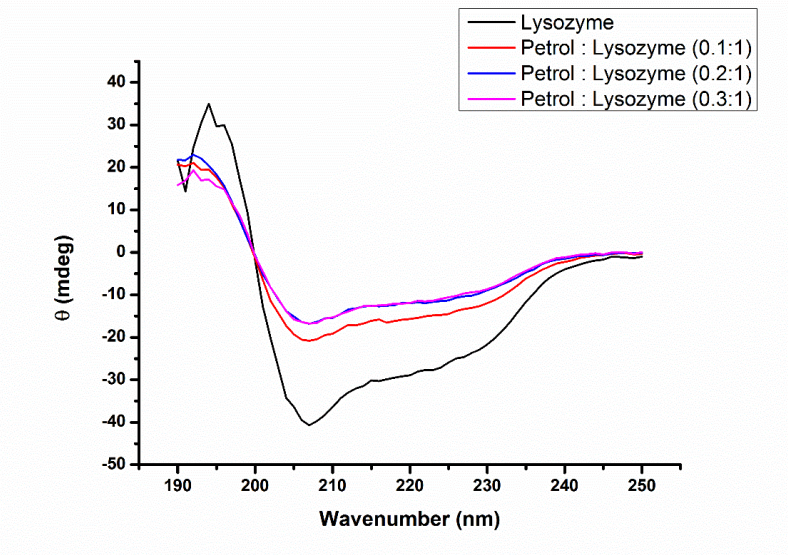

Figure 4-18 CD spectra of GQD treated lysozyme

4.2.10 Effect on Biofilm formation

Under specific environmental conditions many microorganisms' adherer to surfaces either biotic or abiotic by secreting a complex polysaccharides and other biopolymers that form a matrix like structure called a biofilm. We found that increasing concentrations of nanoparticles inhibit the formation of biofilms (Figure 4-18). The inhibitory effect of the GQDs is consistent even when change the strain of the bacteria, indicating that the inhibitory effect is a result of interaction or alteration of a more systemic mechanism common overall multiple species rather than a strain specific mechanism. These results imply that these GQDs, when exposed to a specific region in high concentration, would have an adverse effect the growth of biofilms, which in turn would cause a disruption in the ecological balance.

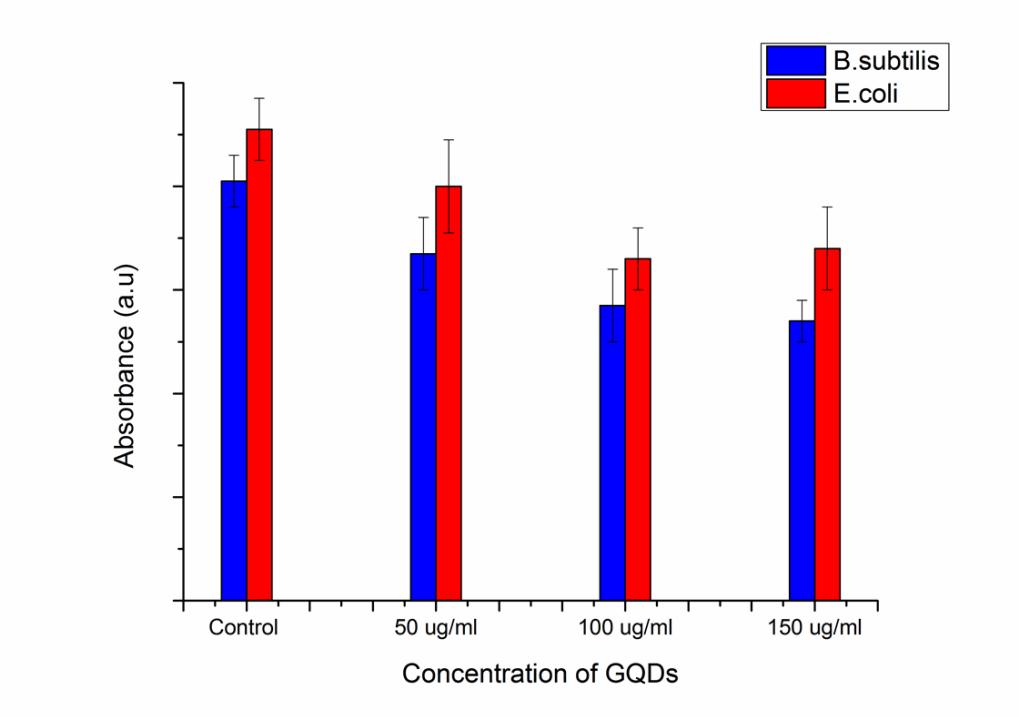

Figure 4-19 Effect of petrol GQD on biofilm formation

4.3 Environmental and long term health impact of GQD

4.3.1 Characterization of Lab synthesized GQD:

The size of graphene quantum dots were characterised using the TEM. The TEM micrographs (Figure 4-19a) clearly show the size of the particles is less than 10 nm. The X-ray diffractrograms of the GQD shoe a characteristic peak at 26^{o} with a d spacing value of 0.34 nm characteristic for the [002] peak of graphite (Figure 4-19e). The FTIR spectroscopy analysis shows the presence of multiple absorbance peaks at 3200 cm^{-1}, 1640 cm^{-1}, 1400 cm^{-1} and 1100cm^{-1}. The UV- visible spectroscopy showed a characteristic peaks at 210 and 280 nm, while the florescence spectroscopy showed that characteristic down conversion of incident light.

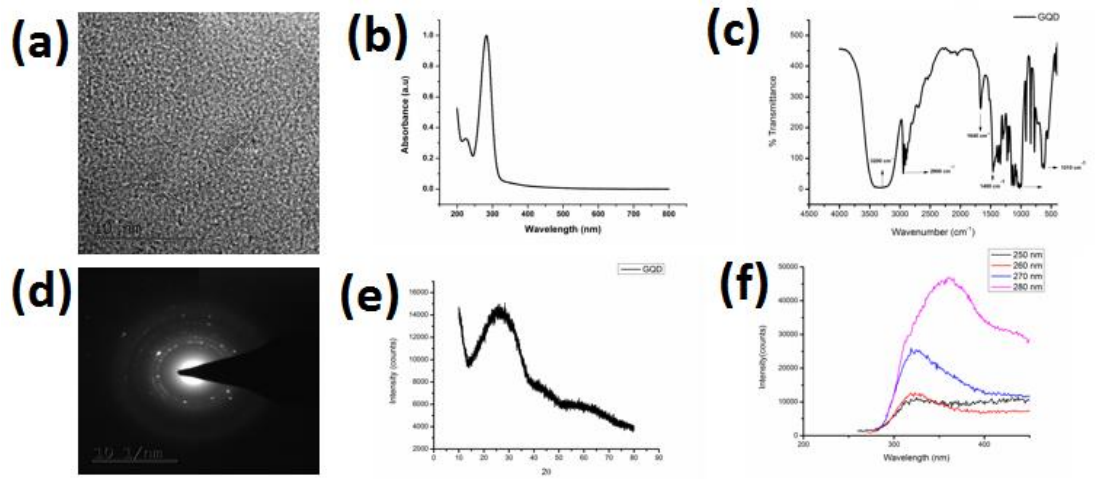

Figure 4-20 Physical characterization of GQD ;(a) HR TEM ;(b) UV Visible spectroscopy ;(c) FTIR of the GQD;(d) SAED analysis of the GQD ;(e) XRD diffract gram of the GQD; (f) PL spectra of the GQD

4.3.2 GQD stabilized Emulsions:

Pickering emulsions were created by dispersing predetermined mass of GQD in water then sonicating them using a bath sonicator for 90s. The ratio of oil: water was kept fixed at 3:7 and hexadecane was used as the oil phase. The light microscopy images showed that particles size of the emulsions varied with the system, while the size of the particles increased with the increasing concentration of the GQD. This heterogeneity in droplet size was more evident in the SEM micrographs, where droplets with diameter varying from a 2 um to 900 nm were observed (Figure 4-20b). Confocal microscopy, allowed us to visualise the distribution of the GQD in the emulsion system, the images showed the GQD were localised at the oil water interface thereby stabilising the emulsion system(Figure 4-20c).

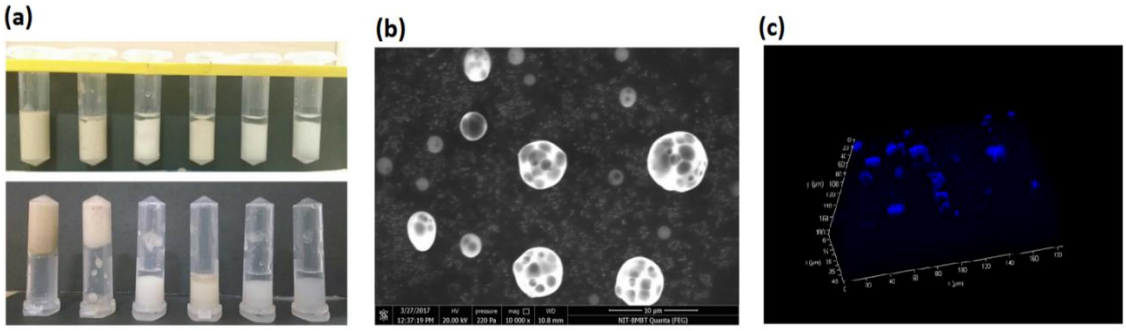

Figure 4-21 (a) Emulsion formed by using different concentration of GQD (50,20,10,5,1,0 mg/ml from right to left respectively); (b) E-SEM micrographs of the GQD stabilised emulsion ; (c)Confocal microscopy images of the Emulsions

The stability of the emulsions was determined by placing exposing them to varying centrifugal forces for different durations of time. The result showed that in terms of centrifugal force beyond 7000 rpm the emulsions tend to destabilise. Similar destabilization was also observed when the duration of centrifugation was increased beyond 4 minutes even at relatively low centrifugation speeds of 5000 rpm.

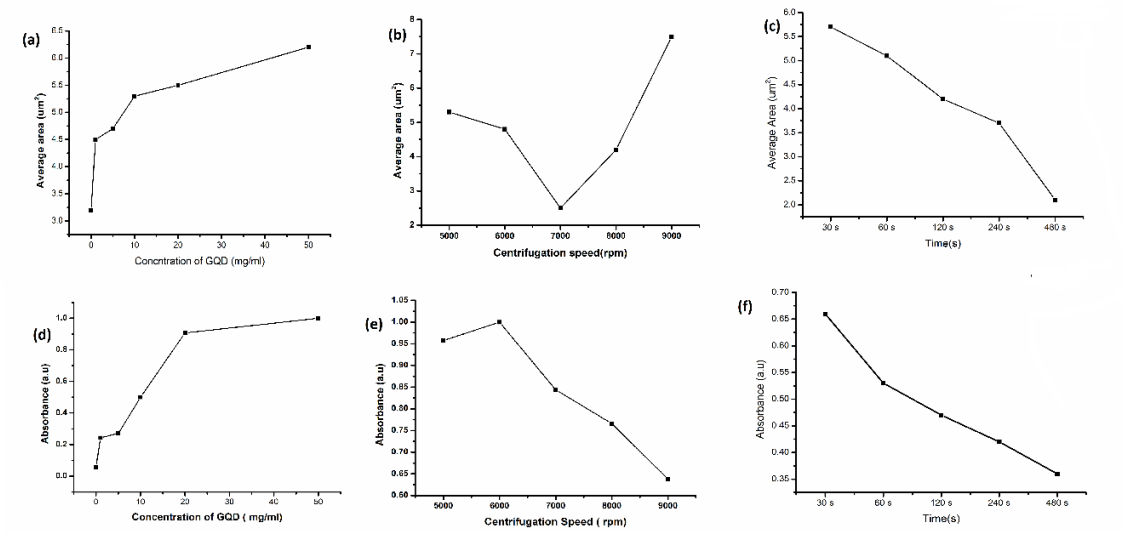

Figure 4-22 Stability analysis of the emulsions (a) variation in size of droplet with increasing GQD concentration;(b) Variation in size of droplets with changing centrifugation speeds ; (c) Variation in size of droplets with changing centrifugation time;(d) change in opacity with carrying GQD concentration;(e) change in opacity with change in centrifugation time.

4.3.3 DSC and Freezing analysis of GQD solutions:

The analysis of the DSC graphs of GQD solution showed a peculiar trend. The latent heat of the 1 mg/ml solution was higher than the latent heat of the 10 mg/ml solution. While both values were higher that the latent heat for pure MIlliQ water this data, shows the presence GQD have an undeniable effect on the freezing rate of the solution (Figure 4-22). The higher latent heat in case of the 1 mg/ml as compared to that of 10 mg/ml solution can be explained by the tendency of GQD at higher concentrations to aggregate. The aggregation ultimately results in a lower number of bonding between

that between the GQD and water molecule as compared to the bonding in case of evenly dispersed GQD, which occurs a low concentration.

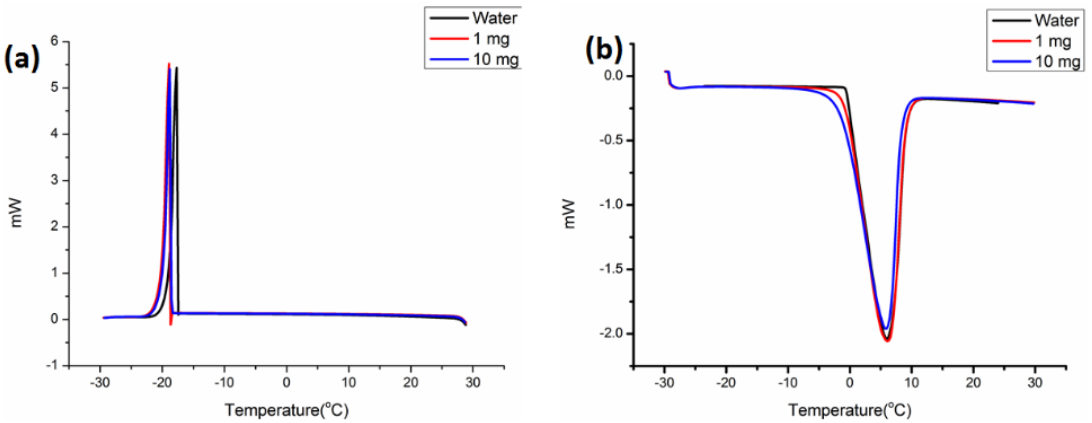

Figure 4-23 DSC graphs of GQD solutions with water as control

The graphs from the cryo probe experiments also showed that the onset temperature of freezing and melting occurred at an earlier time point the GQD samples as compared to the pure water samples (Figure 4-23). It can also be observed that the rate of melting is higher in case of the GQD samples.

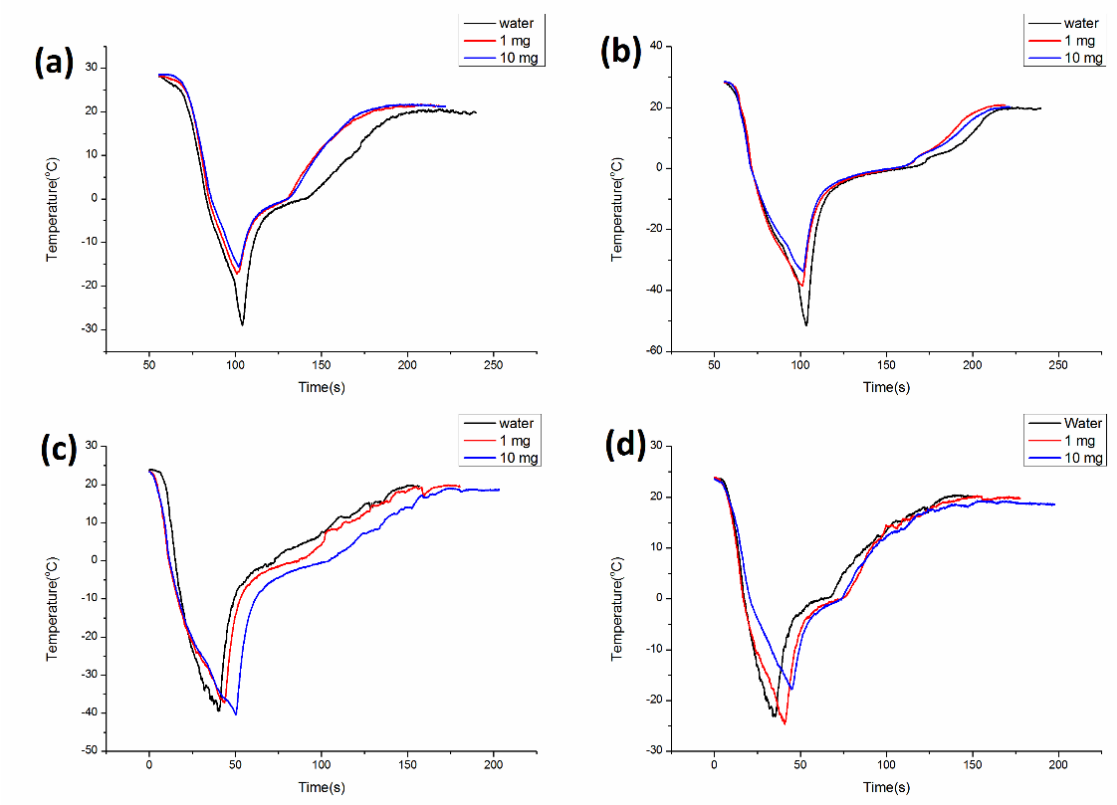

Figure 4-24 Temperature vs Time graphs obtained by using cryoprobe set up (a) and (b) constant time experiments ;(c) and (d) constant temperature experiments

4.3.4 GQD induced calcification:

The PDMS coated with GQD showed a great degree of precipitation of salt; in stark contrast to the complete lack of any discernible precipitation in case of the pure PDMS control samples(Figure 4-24). The presence of large number negatively charged functional groups present on the surface of the GQD particles facilitates the accumulation of positive ions on the surface resulting in the salt precipitation. It was observed from the elemental analysis that the calcium: phosphate ratio was close to 1.43, indicative of the presence of calcium deficit hydroxyapatite. This is significant as this particular form of hydroxyl apatite is generally found in coronary artery calcification.

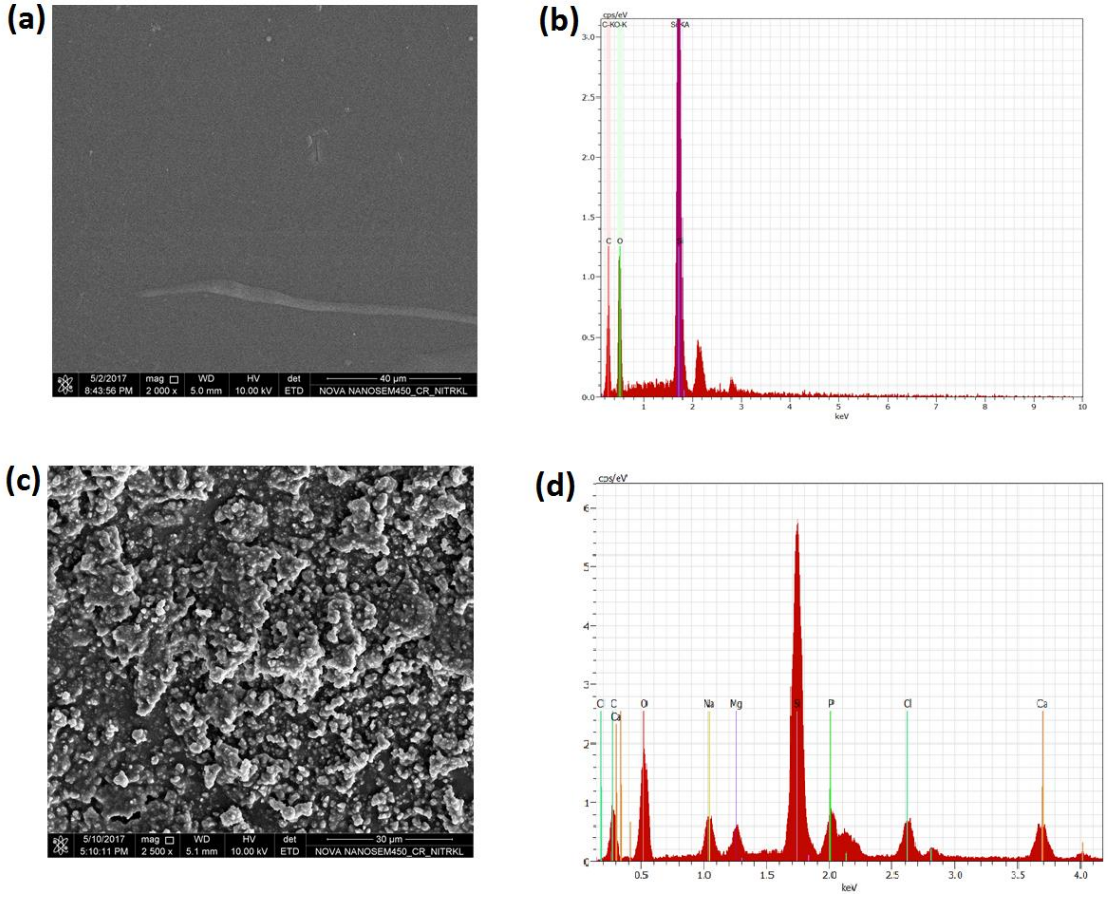

Figure 4-25 (a)&(b) SEM image and EDAX graph respectively of control PDMS film; (c)&(d) the SEM image and EDAX graph of the GQD coated samples.

4.3.5 Vapour phase extraction of GQD:

The GQDs showed an ability to move in the vapour phase when dispersed in certain solvents (Figure 4-24) .This effect was most pronounced in case of solvents such as Acetonitrile, chloroform and butanol, while purely organic solvents such as Hexane and toluene showed no such movement. This process has great potential as a method for the large-scale extraction and purification of GQDs

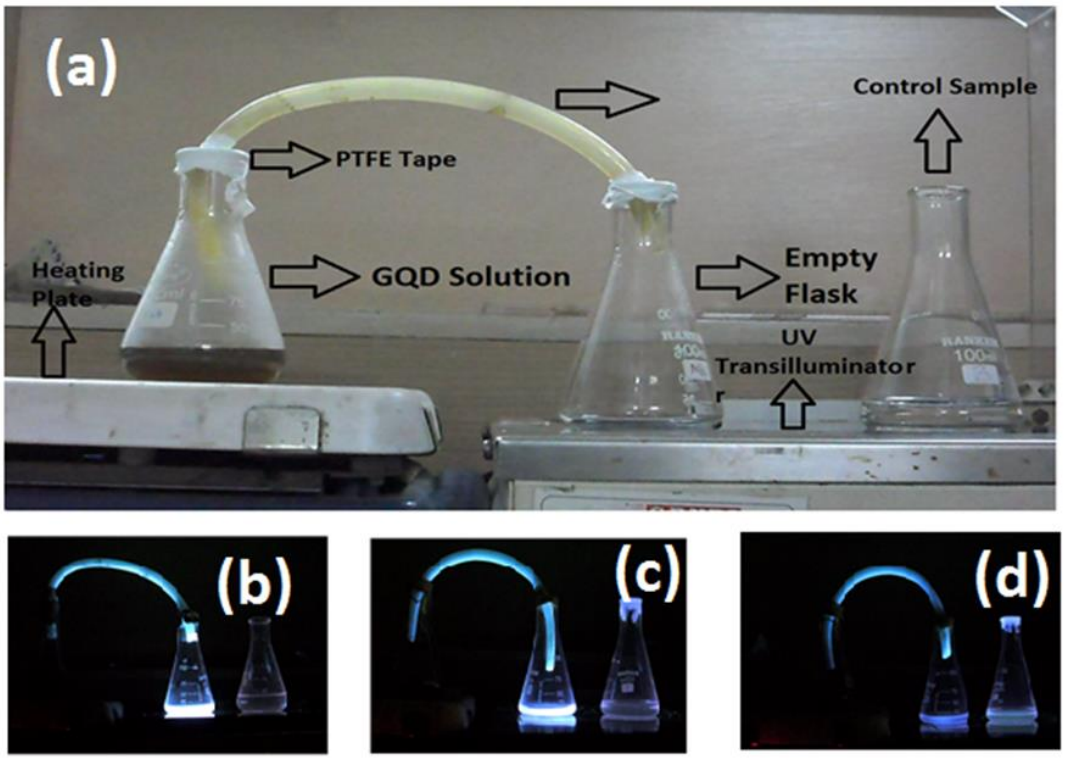

Figure 4-26 :(a) Vapour Phase extraction set up ; (b) extraction in ACN ; (c) extraction in Butanol ; (d) extraction in Chloroform

Chapter 5

Conclusion

The presence of GQD from sources such as cigarette as or exhaust fumes has been hitherto unreported. Further, the presence of these GQDs in the air via expulsion from exhaust pipes or smoke results in them acting as air pollutants. This further implies that there is continuous and extensive exposure to the GQDs in day-to-day life. It is in this regard that the cytotoxicity of the GQD in particular their tendency to generate reactive oxygen species, is highly detrimental to health.

The data also shows that apart for ROS generation the GQDs are also responsible for change in protein structure. This is caused due to the interaction between the functional groups of the GQD and amino acid functional groups. Our preliminary experiments also point towards GQDs have some role in both calcification of coronary artery as well as in the stabilizing body lipids and triglycerides

The effect of GQD on the environment is not just limited to their effect on human health as they have the ability to decrease biofilm formation. While this ability may be useful in context of medical treatment, the formation of biofilms in the natural environment is an essential set in the many key processes such as degradation of Xenobiotic compounds. The effect on the environment is not merely localized to living organisms as the GQD cause a significant depression in the freezing point and change the rate of melting of the water. This data when viewed along side research indicating increased global warming due to pollution from automobiles , allows us to futher understand how we are effect the environment and the setps we need to take to save it.

Thus we need to further understand the both that GQD have both in terms of their cytotoxicity resulting from extended exposure and the effect that their accumulation has on the environment.

Chapter 6

References

1. Wu, C., et al., *Adv. Healthcare Mater., 2013, 2, 1613;(c) SY Lim, W. Shen and ZQ Gao.* Chem. Soc. Rev, 2015. **44**: p. 362.

2. Liu, W.W., et al., *Superior Micro-Supercapacitors Based on Graphene Quantum Dots.* Advanced Functional Materials, 2013. **23**(33): p. 4111-4122.

3. Sun, H., et al., *Deciphering a Nanocarbon-Based Artificial Peroxidase: Chemical Identification of the Catalytically Active and Substrate-Binding Sites on Graphene Quantum Dots.* Angewandte Chemie International Edition, 2015. **54**(24): p. 7176-7180.

4. Hai, X., et al., *An acid-free microwave approach to prepare highly luminescent boron-doped graphene quantum dots for cell imaging.* Journal of Materials Chemistry B, 2015. **3**(47): p. 9109-9114.

5. Tian, X., et al., *Hydroxylated-graphene quantum dots induce cells senescence in both p53-dependent and-independent manner.* Toxicology Research, 2016. **5**(6): p. 1639-1648.

6. Markovic, Z.M., et al., *Graphene quantum dots as autophagy-inducing photodynamic agents.* Biomaterials, 2012. **33**(29): p. 7084-7092.

7. Nurunnabi, M., et al., *In vivo biodistribution and toxicology of carboxylated graphene quantum dots.* ACS nano, 2013. **7**(8): p. 6858-6867.

8. Wu, X., et al., *Fabrication of highly fluorescent graphene quantum dots using L-glutamic acid for in vitro/in vivo imaging and sensing.* Journal of Materials Chemistry C, 2013. **1**(31): p. 4676-4684.

9. Wang, S., I.S. Cole, and Q. Li, *The toxicity of graphene quantum dots.* RSC Advances, 2016. **6**(92): p. 89867-89878.

10. Xu, F., et al., *Masking agent-free and channel-switch-mode simultaneous sensing of Fe 3+ and Hg 2+ using dual-excitation graphene quantum dots.* Analyst, 2015. **140**(12): p. 3925-3928.

11. Dey, S., et al., *Luminescence properties of boron and nitrogen doped graphene quantum dots prepared from arc-discharge-generated doped graphene samples.* Chemical Physics Letters, 2014. **595**: p. 203-208.

12. Shinde, D.B. and V.K. Pillai, *Electrochemical preparation of luminescent graphene quantum dots from multiwalled carbon nanotubes.* Chemistry–A European Journal, 2012. **18**(39): p. 12522-12528.

13. Qu, B., et al., *Layered SnS2-Reduced Graphene Oxide Composite–A High-Capacity, High-Rate, and Long-Cycle Life Sodium-Ion Battery Anode Material.* Advanced materials, 2014. **26**(23): p. 3854-3859.

14. Zhu, S., et al., *The photoluminescence mechanism in carbon dots (graphene quantum dots, carbon nanodots, and polymer dots): current state and future perspective.* Nano Research, 2015. **8**(2): p. 355-381.

15. Qu, G., et al., *Graphene oxide induces toll-like receptor 4 (TLR4)-dependent necrosis in macrophages.* ACS nano, 2013. **7**(7): p. 5732-5745.

16. Wang, R. and F. Zhang, *NIR luminescent nanomaterials for biomedical imaging.* Journal of Materials Chemistry B, 2014. **2**(17): p. 2422-2443.

17. Liao, K.-H., et al., *Cytotoxicity of graphene oxide and graphene in human erythrocytes and skin fibroblasts.* ACS applied materials & interfaces, 2011. **3**(7): p. 2607-2615.

18. Kang, H., et al., *Pharmacokinetics, pharmacodynamics and toxicology of theranostic nanoparticles.* Nanoscale, 2015. **7**(45): p. 18848-18862.

19. Zhao, Y., Q. Wu, and D. Wang, *A microRNAs–mRNAs network involved in the control of graphene oxide toxicity in Caenorhabditis elegans.* RSC Advances, 2015. **5**(112): p. 92394-92405.

20. Qu, G., et al., *Cytotoxicity of quantum dots and graphene oxide to erythroid cells and macrophages.* Nanoscale research letters, 2013. **8**(1): p. 198.

21. Sun, H., et al., *Graphene quantum dots-band-aids used for wound disinfection.* ACS nano, 2014. **8**(6): p. 6202-6210.

22. Fu, P., et al., *A self-assembled chiral-aptasensor for ATP activity detection.* Nanoscale, 2016. **8**(32): p. 15008-15015.

23. Dai, Y., et al., *Versatile graphene quantum dots with tunable nitrogen doping.* Particle & Particle Systems Characterization, 2014. **31**(5): p. 597-604.

24. Li, H., et al., *Tuning laccase catalytic activity with phosphate functionalized carbon dots by visible light.* ACS applied materials & interfaces, 2015. **7**(18): p. 10004-10012.

25. Kundu, S., et al., *Synthesis of N, F and S co-doped graphene quantum dots.* Nanoscale, 2015. **7**(27): p. 11515-11519.

26. Bian, S., et al., *One-pot synthesis of sulfur-doped graphene quantum dots as a novel fluorescent probe for highly selective and sensitive detection of lead (II).* RSC Advances, 2016. **6**(74): p. 69977-69983.

27. Song, Z., et al., *Multifunctional N, S co-doped carbon quantum dots with pH- and thermo-dependent switchable fluorescent properties and highly selective detection of glutathione.* Carbon, 2016. **104**: p. 169-178.

28. Wang, Y., et al., *Fluorescent polyvinyl alcohol films based on nitrogen and sulfur co-doped carbon dots towards white light-emitting devices.* New Journal of Chemistry, 2016. **40**(10): p. 8710-8716.

29. Sun, Y., et al., *Correction: Facile synthesis of biocompatible N, S-doped carbon dots for cell imaging and ion detecting.* RSC Advances, 2015. **5**(27): p. 20691-20691.

30. Patel, M.A., et al., *P-Doped Porous Carbon as Metal Free Catalysts for Selective Aerobic Oxidation with an Unexpected Mechanism.* ACS nano, 2016. **10**(2): p. 2305-2315.

31. Gong, Y., et al., *Phosphorus, and nitrogen co-doped carbon dots as a fluorescent probe for real-time measurement of reactive oxygen and nitrogen species inside macrophages.* Biosensors and Bioelectronics, 2016. **79**: p. 822-828.

32. AshaRani, P., et al., *Cytotoxicity and genotoxicity of silver nanoparticles in human cells.* ACS nano, 2008. **3**(2): p. 279-290.